Available online at www.sciencedirect.com
ScienceDirect
Journal of the European Ceramic Society 31 (2011) 2663–2669
www.elsevier.com/locate/jeurceramsoc

Processing and performance of solid oxide fuel cell with Gd-doped ceria electrolyte

Yuta Ibusuki, Hajime Kunigo, Yoshihiro Hirata *, Soichiro Sameshima, Naoki Matsunaga

Department of Chemistry, Biotechnology, and Chemical Engineering, Kagoshima University, 1-21-40 Korimoto, Kagoshima 890-0065, Japan

Available online 16 February 2011

Abstract

Fuel Cell performance was measured at 792–1095 K for Ni-GDC (Gd-doped ceria) anode-supported GDC film (60 μm thickness) with a $(La_{0.8}Sr_{0.2})(Co_{0.8}Fe_{0.2})O_3$ cathode using H_2 fuel containing 3 vol% H_2O. A maximum power density, 436 mW/cm^2, was obtained at 1095 K. The electrical conductivity of GDC electrolyte in N_2 atmosphere of 10^{-15}–10^0 Pa oxygen partial pressures (Po_2) at 773–1073 K was independent of Po_2, which indicated the diffusion of oxide ions. The conductivity of GDC in H_2O/H_2 atmosphere increased because of the further formation of electrons due to the dissociation of hydrogen in GDC ($H_2 \rightarrow 2H^+ + 2e^-$). The hole conductivity was observed at 873 K in $Po_2 = 10^0$–10^4 Pa. The key factors in increasing power density are the increase of open circuit voltage and the suppression of H_2 fuel dissolution in GDC electrolyte. These are controlled by the cathode material and Gd-dopant composition.

Keywords: C. Electrical properties; C. Ionic conductivity; D. CeO_2; E. Fuel cells; Open circuit voltage

1. Introduction

Reducing the operating temperature of solid oxide fuel cells (SOFC) expands the choice of cell materials and increases the operating life of SOFCs.[1] Rare earth-doped ceria (RDC) has a high oxide ion conductivity and can be added to a SOFC electrolyte. However, Ce^{4+} ions and lattice oxygen ions react in RDC to form Ce^{3+} ions, positively charged oxide ion vacancy, electrons and oxygen molecules at a low oxygen partial pressure.[2,3] The formation of electrons in RDC electrolyte decreases open circuit voltage (OCV) of a cell, resulting in a decreased power density.[4–6] In our previous paper,[7] we detailed the processing and cell performance of anode-supported Gd-doped ceria films (GDC, $Ce_{0.8}Gd_{0.2}O_{1.9}$, 30 μm thick) with a $SrRuO_3$ cathode. The maximum power densities measured were 100 mW/cm^2 at 873 K and 380 mW/cm^2 at 1073 K when the cell was supplied with H_2 fuel. However, the OCV of the cell was low when compared with the value calculated by the Nernst equation with no electronic conduction or the calculated value for the mixed conductor of oxide ions and electrons calculated by the Hebb–Wagner method. The decrease in OCV was significant for thinner GDC film. This was presumed to be caused by the dissolution and dissociation of H_2 fuel in the GDC film to form protons and electrons ($H_2 \rightarrow 2H^+ + 2e^-$).[8] This reaction occurs due to oxide ion vacancy ($H_2 + V_O^{\bullet\bullet} \rightarrow 2H^+ + V_O^\times$, $V_O^\times \rightarrow V_O^{\bullet\bullet} + 2e^-$). The decrease of overpotential at the cathode may be an effective strategy to prevent the dissolution of hydrogen in a GDC film, because the overpotential at the anode is generally lower than that at the cathode. When the flux of oxide ions in the GDC film is significantly higher than the flux of dissolved hydrogen, it is possible to maintain a high terminal voltage. In this paper, the cell performance of a Ni-GDC anode-supported GDC cell (composed of $Ce_{0.8}Gd_{0.2}O_{1.9}$) with a $(La_{0.8}Sr_{0.2})(Co_{0.8}Fe_{0.2})O_3$ cathode[7] was measured at 792–1095 K to compare with the power density of a GDC cell with a $SrRuO_3$ cathode and the reported power density of a GDC cell (composed of $Ce_{0.9}Gd_{0.1}O_{1.95}$) with a $(La_{0.8}Sr_{0.2})(Co_{0.8}Fe_{0.2})O_3$ cathode.[9] Furthermore, the electrical conductivity of Gd-doped ceria electrolyte was measured in air, N_2 atmosphere and H_2O/H_2 atmosphere to identify the dominant migration species (oxide ions, holes, electrons and protons) in a wide oxygen pressure range. Based on the experimental results, it was clear that the electric power of a GDC cell can be increased by using a $(La_{0.8}Sr_{0.2})(Co_{0.8}Fe_{0.2})O_3$ cathode rather than a $SrRuO_3$ cathode and by decreasing the Gd content from $x = 0.2$ to 0.1 in the $Ce_{1-x}Gd_xO_{2-(x/2)}$ composition. The

* Corresponding author. Tel.: +81 99 285 8325; fax: +81 99 257 4742.
E-mail address: hirata@apc.kagoshima-u.ac.jp (Y. Hirata).

0955-2219/$ – see front matter © 2011 Elsevier Ltd. All rights reserved.
doi:10.1016/j.jeurceramsoc.2011.01.020

above factors allow a high OCV and a high current density for the cell with H_2 fuel.

2. Experimental procedure

2.1. Preparation of cell materials

The detailed preparation method for the GDC powder is reported in our previous paper.[10] The GDC precursor, oxalate solid solution $(Ce_{0.8}Gd_{0.2})_2(C_2O_4)_3$, was prepared by placing the mixed nitrate solution (0.2 M) of Ce and Gd into 0.4 M oxalic acid solution. The produced coprecipitate was decomposed to GDC at 873 K in air. The obtained GDC powder was ball-milled for 24 h. Non-aqueous GDC suspensions of 25 vol% solids were prepared using a mixed solution of 33 vol% toluene and 67 vol% isopropanol. Nine mass% of polyethyleneglycol and 5 mass% of polyvinyl butyral were added to the milled GDC powders.[7,8] The suspensions were consolidated on a polyester sheet with a doctor blade (DP-100, Tsugawa Seiki Seisakusho, Tokyo). Furthermore, the milled GDC powder was then immersed into a 1.4 M $Ni(NO_3)_2$ solution to make a Ni-GDC anode with a volume ratio of Ni/GDC = 40/60. The suspension was freeze-dried and calcined at 873 K for 1 h in air. $(La_{0.8}Sr_{0.2})(Co_{0.8}Fe_{0.2})O_3$ cathode powder (LSCF) was prepared by heating the freeze-dried coprecipitation of $La(NO_3)_3$, $Sr(NO_3)_2$, $Co(NO_3)_2$ and $Fe(NO_3)_3$ with $(NH_4)_2CO_3$.[9,11] The freeze-dried powder was calcined at 1173 K for 2 h in air and the produced solid a solution was identified by X-ray diffraction (RINT2200, Rigaku Denki Co. Ltd., Japan).

The GDC film was placed on a NiO-GDC powder bed (22 mm diameter, 2 mm thickness) to form a porous structure and compressed uniaxially at 50 MPa, followed by isostatic pressing at 294 Pa. The compacts were heated at 1673 K for 4 h in air. The thickness of the resulting GDC electrolyte was 60 μm. The LSCF powders were dispersed at 15 vol% solid in a mixed solution of 90 vol% ethanol and 10 vol% ethyleneglycol. This suspension was spread over the GDC electrolyte on a NiO-GDC anode by screen printing (70 μm mesh, 4 mm diameter), and heated at 1173 K for 1 h in air. The thickness of the attached cathode layer was 100 μm.

2.2. Measurement of cell performance

A Pt wire was attached to the electrodes of the GDC cell. The GDC electrolyte with the cathode and anode was placed on an alumina holder and sealed at 1173 K with a glass O-ring. The NiO at the anode was reduced to Ni by reacting with the H_2 fuel containing 3 vol% H_2O ($NiO + H_2 \rightarrow Ni + H_2O$) at 1073 K. After it cooled to 1095, 1006, 906 and 792 K, the cell performance was measured by feeding air at 100–500 ml/min into the cathode and H_2 fuel containing 3 vol% H_2O at 100 ml/min into the anode. The oxygen partial pressure of the fuel was monitored with an yttria-stabilized zirconia (YSZ) oxygen gas sensor.

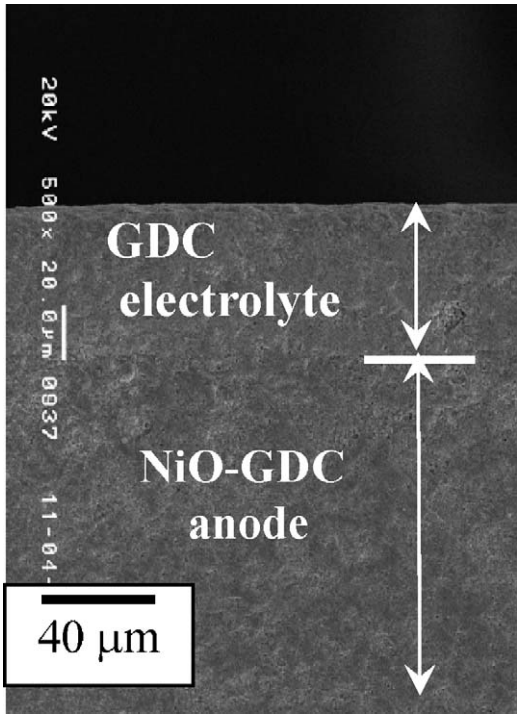

Fig. 1. Cross-section of NiO-GDC anode-supported GDC electrolyte sintered in air at 1673 K.

2.3. Electrical conductivity measurement

The GDC powder produced in Section 2.1 was ball-milled for 24 h and then pressed isostatically at 294 MPa to form a disk of 10 mm diameter and 2 mm thickness. The disk was sintered at 1773 K for 4 h in air to obtain a GDC disk with 96–98% theoretical density. The electrical conductivity of the GDC disk in air, N_2 atmosphere and H_2O/H_2 atmosphere at 773–1073 K was measured with a two-terminal AC bridge circuit using a self-inductance–capacitance–impedance (LCZ) meter (100 Hz to 2 MHz, model 4194A, Agilent Technologies Co.) and also using the two-terminal DC method with a potentiometer (HA-510G, Hokuto Denko Co., Japan). Pt paste was spread homogenously on the planes of GDC, polished with 1 μm diamond paste and heated at 1123 K for 2 h to create Pt electrodes. The oxygen partial pressure range in the N_2 gas was controlled from 1 Pa to 10^{-15} Pa by passing N_2 gas into an oxygen pump using a YSZ electrolyte (KOC-200B, Kaken Inc., Ibaraki, Japan). The oxygen partial pressure in H_2 containing 3 vol% H_2O gas was monitored with a YSZ oxygen sensor.

3. Results and discussion

3.1. Cell performance with anode-supported GDC electrolyte

Fig. 1 shows the cross section of the Ni-GDC anode-supported GDC electrolyte. The dense GDC film (60 μm thickness) was firmly adhered to a NiO-GDC anode by sintering in air at 1673 K. In our previous work,[7] increasing the thickness of the NiO-GDC anode was effective in decreasing the warp

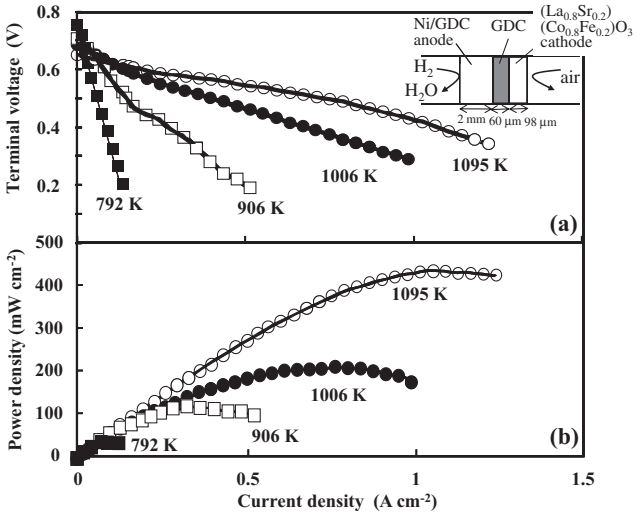

Fig. 2. (a) Terminal voltage and (b) electric power density as a function of current density at 792−1095 K for anode-supported cell with 60 μm GDC film covered with porous $(La_{0.8}Sr_{0.2})(Co_{0.8}Fe_{0.2})O_3$ cathode.

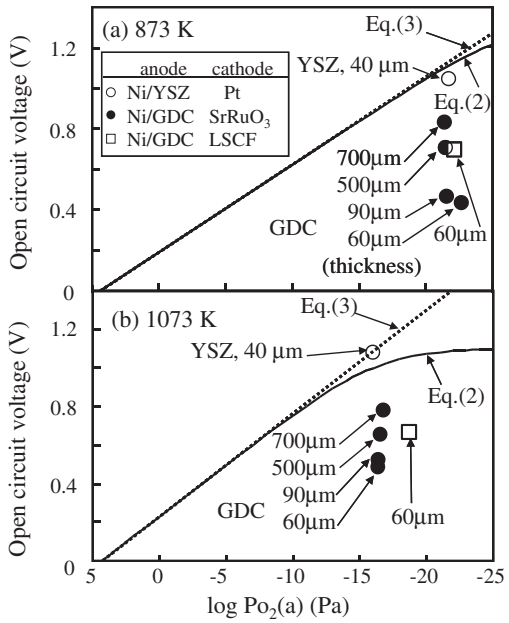

Fig. 3. OCV measured for GDC and YSZ films at (a) 873 and (b) 1073 K as a function of oxygen partial pressure at anode. The dotted and solid lines represent Eqs. (3) and (2) in text, respectively, and correspond to OCV of GDC without and with electronic conduction in an atmosphere without H_2 molecules, respectively.

and in increasing the sintered density of the laminated cell. A similar good adhesion without warp was achieved between the GDC electrolyte and the anode in this study.

Fig. 2 shows the (a) terminal voltage and (b) electric power density as a function of the current density at 792–1095 K for a cell with a Ni-GDC anode (2 mm thickness), GDC electrolyte (60 μm thickness) and a LSCF8282 cathode (100 μm thickness). The OCV was 0.741, 0.711, 0.695 and 0.652 V at 792, 906, 1006 and 1095 K, respectively. The theoretical OCV calculated by the Nernst equation was 1.135, 1.126, 1.098 and 1.058 V for an anode with 2.17×10^{-25}, 1.83×10^{-21}, 2.11×10^{-18} and 6.94×10^{-16} Pa oxygen partial pressure at 792, 906, 1006 and 1095 K, respectively. The measured OCV was lower than the calculated OCV. This is due to the electronic conduction of GDC electrolyte at a low oxygen partial pressure and discussed in a later part of this section. The maximum powder density was 32, 117, 209 and 436 mW/cm^2 at 792, 906, 1006 and 1095 K, respectively.

Fig. 3 shows the OCV of an anode supported-GDC cell at (a) 873 K and (b) 1073 K.[8] In an open circuit, the summation of $J(O^{2-})$ and $J(e)$ (J: flux of oxide ions and electrons) is zero (Eq. (1)), and the OCV is calculated by Eq. (2),

$$\left|J(O^{2-})\right| = |J(e)| = \frac{nRT}{4FL}\sigma(O^{2-}) \ln\left[\frac{\sigma(O^{2-}) + KPo_2(c)^{-1/n}}{\sigma(O^{2-}) + KPo_2(a)^{-1/n}}\right] \quad (1)$$

$$E = \varphi(c) - \varphi(a) = \frac{nRT}{4F} \ln\left[\frac{Po_2(c)^{1/n} + \{K/\sigma(O^{2-})\}}{Po_2(a)^{1/n} + \{K/\sigma(O^{2-})\}}\right] \quad (2)$$

where R is the gas constant, F is the Faraday constant, L is the thickness of the electrolyte, T is the temperature, K and n are the constants where the electronic conductivity $\sigma_e = KPo_2^{-1/n}$, $Po_2(c)$ and $Po_2(a)$ are the oxygen partial pressures at the cathode and anode, respectively, $\sigma(O^{2-})$ is the oxide ion conductivity, and $\varphi(c)$ and $\varphi(a)$ are the electric potential at the cathode and anode respectively. When a mixed conductor has no electronic conduction ($K = 0$), $J(O^{2-})$ and $J(e)$ are zero, which indicates that there is no transportation of oxide ions or electrons. The OCV for $K = 0$ is given by Eq. (3), which is known as the Nernst equation.

$$E_N(K = 0) = \frac{RT}{4F} \ln\left(\frac{Po_2(c)}{Po_2(a)}\right) \quad (3)$$

From Eqs. (1) to (3), the OCV of a mixed conductor is related to the internal short circuit current ($J = |J(O^{2-})| = |J(e)|$) with Eq. (4).

$$E = E_N - \left(\frac{L}{\sigma(O^{2-})}\right) J \quad (4)$$

The OCV of an yttria-stabilized zirconia cell was very close to the Nernst equation (Eq. (3)), which indicated that the electronic conduction ($J = 0$) was negligible.[8] The OCV of the GCD film decreased as the film was thinner, which indicated an increased J value (Eq. (4)) with the decreased thickness. Furthermore, the measured OCV of a GDC electrolyte cell using H_2 fuel was lower than the OCV calculated by Eq. (2) using K and n values measured by the Hebb–Wagner method in N_2 atmosphere.[12] The reason for this is reported in the Introduction and is due to the formation of electrons when H_2 fuel reacts with oxide ion vacancy. An LSCF8282 cathode for the GDC electrolyte provided a higher OCV than a $SrRuO_3$ cathode for the GDC electrolyte, which indicated a decrease of internal short circuit current of the mixed conductor. It is possible to increase the OCV of the mixed conductor by decreasing the overpotential at the cathode.

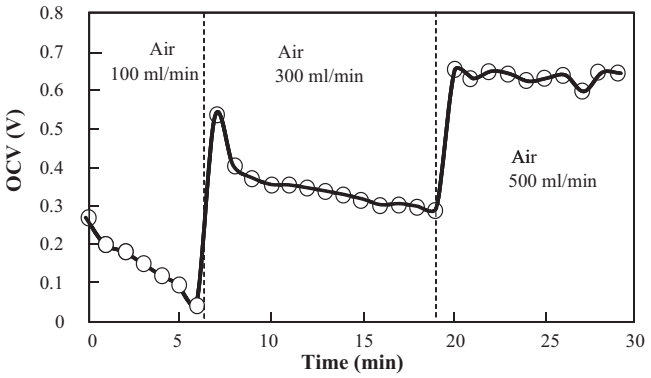

Fig. 4. Open circuit voltage (OCV) of GDC cell with LSCF8282 cathode at 1095 K as a function of flow rate of air.

Fig. 4 shows how the OCV changes with the flow rate of air. The decrease of the OCV of the mixed conductor is due to the decrease of oxygen partial pressure over time in the cathode layer. The oxygen molecules in the cathode react with electrons and are transported to the anode through the GDC electrolyte as oxide ions ($O_2 + 4e^- \rightarrow 2O^{2-}$). When the flow rate of oxygen molecules into the cathode layer is lower than the flow rate of air, the oxygen partial pressure inside the cathode layer decreases, causing a decrease of the OCV. The OCV increased as the flow rate of air increased. The saturated OCV was achieved at a flow rate of 500 ml/min for an LSCF cathode and 200 ml/min for a $SrRuO_3$ cathode.[8] This result suggests that the flow rate of oxygen molecules through GDC electrolyte is higher for LSCF cathode than for $SrRuO_3$ cathode.

Fig. 5 summarizes (a) OCV, (b) current density at the maximum power density (MPD) and (c) MPD for Ni-GDC anode-supported GDC cells. When the cathode was changed from $SrRuO_3$ (sample 3) to LSCF (samples 1 and 2), the OCV increased over a wide operational temperature range. This increased OCV is due to the increased flux of oxide ions. The available current density was significantly higher for a cell with LSCF.[9] In two cells (samples 2 and 3), the cell with a $SrRuO_3$ cathode provided a higher current density than the cell with a LSCF cathode. As a result, these two variables (OCV and current density) were effective when combined to provide a similar

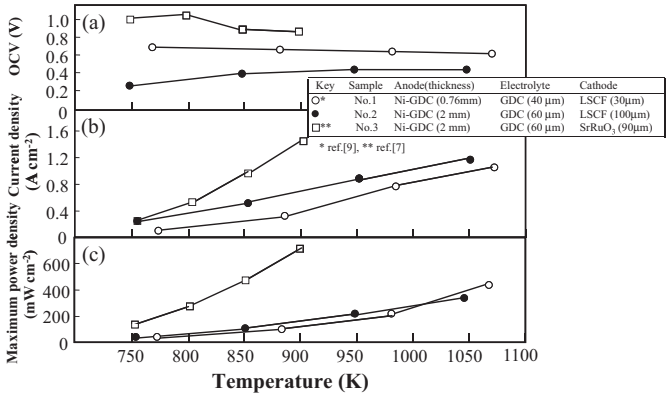

Fig. 5. (a) OCV, (b) current density corresponding maximum power density (MPD), and (c) MPD for Ni-GDC anode-supported GDC cells as a function of operation temperature.

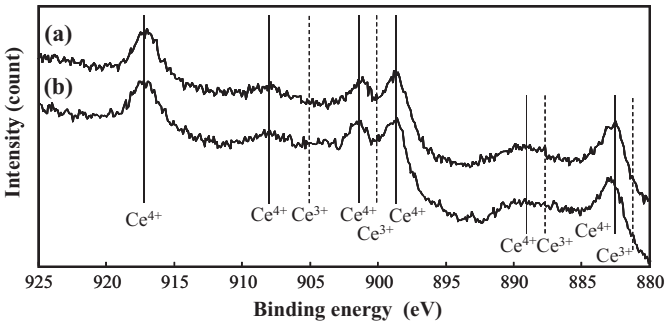

Fig. 6. XPS Ce 3d emission spectra of (a) GDC electrolyte with $Ce_{0.9}Gd_{0.1}O_{1.95}$ composition and (b) GDC electrolyte with $Ce_{0.8}Gd_{0.2}O_{1.9}$ composition.

electric power density for cells Nos. 2 and 3 in Fig. 5(c). Therefore, both the OCV and current density should be increased to achieve a higher power density.

In Ref. [9], GDC electrolyte was prepared from a commercial powder (composed of $Ce_{0.9}Gd_{0.1}O_{1.95}$, Anan Kasei Co. Ltd., Japan, shortened as GDC-A). The amount of Gd-dopant was different from the amount of Gd-dopant in this study (composed of $Ce_{0.8}Gd_{0.2}O_{1.9}$, shortened as GDC-K), but similar XRD profiles were measured. The specific surface areas and equivalent particle sizes for GDC-A were 49.9 m^2/g and 23 nm and for GDC-K were 27.6 m^2/g and 30 nm. Fig. 6 shows the XPS Ce 3d emission spectra of GDC-A and GDC-K films sintered at 1673 K in air. The peaks at 917, 908, 901, 899, 889 and 883 eV were assigned to Ce^{4+} ions.[13,14] The peaks at 905, 900, 887 and 882 eV were assigned to Ce^{3+} ions. As seen in Fig. 6, no significant difference was observed for the two spectra, which suggested the coexistence of Ce^{3+} ions and Ce^{4+} ions in both GDC electrolytes. The coexistence of Gd^{3+} ions and Ce^{3+} ions produces oxide ion vacancy as shown by Eq. (5).

$$Gd_2O_3 \xrightarrow{2CeO_2} 2Gd'_{Ce} + 3O_O^{\times} + V_O^{\bullet\bullet} \quad (5)$$

$$V_O^{\bullet\bullet} + \frac{1}{2}O_2 \rightarrow O_O^{\times} + 2h^{\bullet} \quad (6)$$

$$Ce_2O_3 + V_O^{\bullet\bullet} + \frac{1}{2}O_2 \rightarrow 2Ce'_{Ce} + 4O_O^{\times} + 2h^{\bullet} \rightarrow 2Ce_{Ce}^{\times} + 4O_O^{\times} \quad (7)$$

The oxide ion vacancies formed by the substitution of Gd^{3+} and Ce^{3+} ions for Ce^{4+} ions react with oxygen molecules in the cathode to form holes (Eq. (6)). Therefore, Ce_2O_3 in GDC electrolyte can coexist with holes (Eq. (7)). The high reactivity of Ce^{3+} ions and holes (high stability of Ce^{4+} ions) results in a high OCV and may be due to the Gd content of the GDC electrolyte, the temperature or the oxygen partial pressure. In the anode side of a GDC cell, H_2 fuel dissolves into the GDC electrolyte to form protons, resulting in the increase of electronic conduction (a decrease of OCV) as described in the Introduction. However, the OCV for a $Ce_{0.9}Gd_{0.1}O_{1.95}$ cell in Fig. 5(a) is higher than that for a $Ce_{0.8}Gd_{0.2}O_{1.9}$ cell. This indicates that a decrease of the amount of Gd dopant is effective for creating a higher OCV when the cell is supplied with H_2 fuel. Decreasing the oxide ion

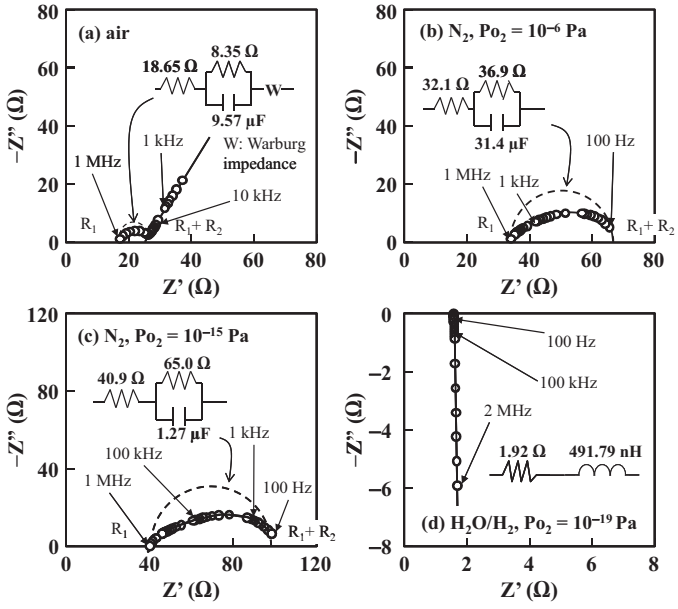

Fig. 7. Complex impedance plots of GDC electrolyte at 873 K in (a) air, (b and c) N_2 atmosphere and (d) H_2O/H_2 atmosphere.

vacancy from $x = 0.2$ to 0.1 in $Ce_{1-x}Gd_xO_{2-(x/2)}$ contributes to the suppression of interaction between H_2 molecules and oxide ion vacancy. The results in Fig. 5 suggest that the combination of the cathode material (LSCF) and the Gd composition of a GDC cell ($Ce_{0.9}Gd_{0.1}O_{1.95}$) is effective in increasing power density. Another strategy to increase the power density is to use the fuel other than H_2 gas such as CH_4, C_2H_6 or C_3H_8 gas, which may not dissolve in GDC electrolyte. Hibino et al. supplied hydrocarbon fuels (CH_4, C_2H_6 and C_3H_8) into SOFCs using a $Ce_{0.9}Gd_{0.1}O_{1.95}$ electrolyte with an anode containing Ru. The OCV and maximum power density at 873 K with dry CH_4 were comparable to H_2 fuel containing 2.9 vol% H_2O.[15] This allows GDC electrolyte to have a high power density with different fuels.

3.2. Electrical conductivity of GDC electrolyte

3.2.1. Complex impedance and conductivity-applied voltage relation

Typical complex impedance plots of GDC at 97.3% of theoretical density and average grain size of 4.93 μm at 873 K are shown in Fig. 7. The plotted impedance of GDC electrolyte in air and N_2 atmosphere formed a distorted semicircle, which suggested a multi-relaxation mechanism of charged species. The dotted lines represent the approximated series circuit of resistance (R_1) plus the parallel circuit of resistance (R_2) and the capacitance. The resistance R_1 (Fig. 7(a–c)) in the high frequency range represents the bulk resistance and the resistance R_2 in the low frequency range represents the grain boundary resistance. In an H_2O/H_2 atmosphere, it was not possible to separate the sample resistance (R) into the bulk resistance and grain boundary resistance. Similarly, the impedance plots at 973–1073 K in air and N_2 atmosphere could not be separated into the bulk resistance and grain boundary resistance.

The relation between the direct current and applied voltage was nonlinear in air and N_2 atmosphere, and linear in an H_2O/H_2 atmosphere. Fig. 8 shows the logσ (conductivity) $-$ E (applied voltage) relation in (a) air at 773–1073 K and in (b) N_2 atmosphere at 10^{-15} to 1 Pa oxygen partial pressure at 873 K. The σ values were derived from the I(current) $-$ E relation at the interval of $\Delta E = 20$ mV as follows: $\sigma = (\Delta I/\Delta E)L/A$, where L is the thickness of the electrolyte and A is the surface area of the electrode. Logσ was low initially when a low voltage was applied and increased at a higher applied voltage, and approached a constant value. The final constant σ value was close to the AC conductivity. The difference of electrical conductivities between the AC and DC measurements is due to the overpotential for the $1/2O_2 + 2e^- \rightarrow O^{2-}$ reaction at the cathode. In this discussion, the overpotential at the anode is ignored to clarify the results. According to the Butler–Volmer model, the conductivity at the cathode is expressed by Eq. (8),

$$\sigma = L\left(\frac{di}{dE}\right) = \left(-\frac{4L\beta F^2 k_- C_O}{RT}\right)\exp\left(-\frac{2\beta FE}{RT}\right) - \left(\frac{4L(1-\beta)F^2 k_+ C_R}{RT}\right)\exp\left(\frac{2(1-\beta)FE}{RT}\right) \quad (8)$$

where i is the difference between the current density of the cathodic reaction ($1/2O_2 + 2e^- \rightarrow O^{2-}$) and the anodic reaction ($O^{2-} \rightarrow 1/2O_2 + 2e^-$), β is the symmetry factor ($0 < \beta < 1$), k_- and k_+ represent the rate constants for the cathodic reaction and the anodic reaction under no applied voltage, respectively, and C_O and C_R are the concentrations of O atoms and oxide ions on the cathode surface, respectively. Eq. (8) provides the minimum σ where $E(\min) = (RT/2F)\ln[\beta k_- C_O/(1-\beta)k_+ C_R]$. Log$\sigma$ decreases linearly with increasing applied voltage where $E < E$ (min) and increases linearly with increasing applied voltage where $E > E$ (min). This Butler–Volmer model explains the measured logσ $-$ E relation well. The DC conductivity at a high applied voltage ($E \approx 2$ V) in Fig. 8 agreed with the AC conductivity and contained no interfacial resistance associated with the chemical reaction at the cathode.

3.2.2. Influence of oxygen partial pressure on electrical conductivity

Fig. 9 shows the conductivity of GDC electrolyte as a function of oxygen partial pressure at 873 K. The bulk, grain boundary and total conductivities of GDC electrolyte measured by the AC method were independent of the oxygen partial pressure in the range of $-15 < \log P_{O_2}$ (Pa) < 0, which suggested there was diffusion of oxide ions. In the calculation of the grain boundary conductivity, the thickness of one grain boundary was determined to be 3 nm from the capacitance in complex impedance plots data in our previous paper.[16] The DC conductivity at 1 V includes the interfacial resistance associated with the chemical reaction at the electrodes. As a result, the DC conductivity was lower than the AC conductivity but independent of the oxygen partial pressure. This result is also explained by the diffusion of oxide ions. An increase of AC and DC conductivities was measured in air and in H_2O/H_2 atmosphere. In Fig. 9, the electronic conductivity of La-doped ceria (LDC) calculated by the

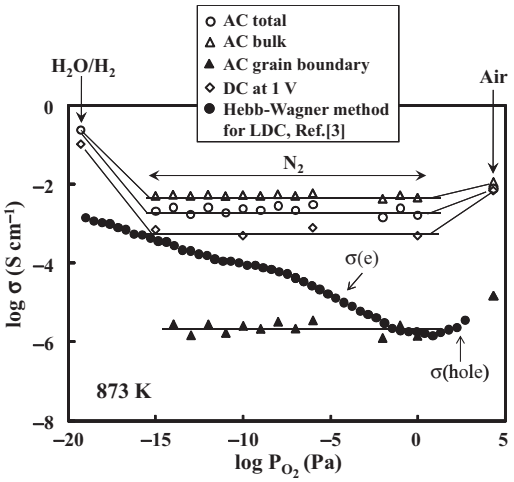

Fig. 9. Influence of oxygen partial pressure on electrical conductivities of GDC at 873 K.

Hebb–Wagner method is also shown.[3] The conductivity of LDC at $0 < \log P_{O_2}\,(\mathrm{Pa}) < 5$ corresponds to the hole conduction and is close to the grain boundary conductivity of GDC electrolyte as calculated by the AC method. The above comparison suggests that the hole conductivity as calculated by the Hebb–Wagner method reflects the hole conduction mainly through the grain boundary. A similar hole conduction is expected from bulk conductivity when the GDC electrolyte sample is set in air. The difference between grain boundary conductivity as calculated by the AC method and electronic conductivity as calculated by the Hebb–Wagner method at $-15 < \log P_{O_2}\,(\mathrm{Pa}) < 0$ is due to the difference of migration species. The present AC data of the grain boundary includes the information of both oxide ions and electrons. The measured result indicates that the resistance of oxide ions is less than the resistance of electrons at the grain boundary. In an H_2O/H_2 atmosphere, the conductivity was increased. This suggests electrons formed by the dissociation of H_2 molecules in GDC electrolyte (Eq. (9)) are contributing in addition to the reaction between Ce^{4+} ions and lattice oxygen ions (Eqs. (10) and (11)).

$$H_2 \rightarrow 2H^+ + 2e^- \tag{9}$$

$$Ce_{Ce}^{\times} + O_O^{\times} \Leftrightarrow Ce_{Ce}' + V_O^{\bullet\bullet} + e^- + \frac{1}{2}O_2 \tag{10}$$

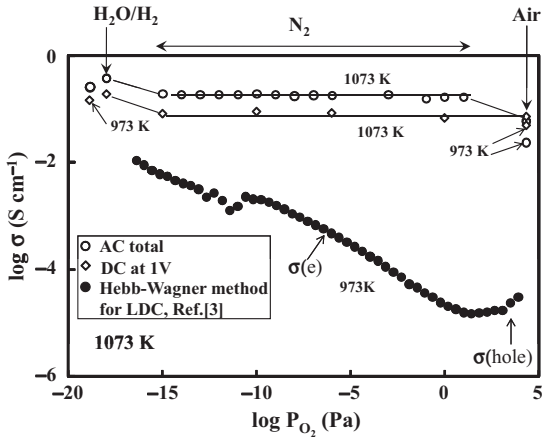

Fig. 10. Influence of oxygen partial pressure on electrical conductivities of GDC at 973 and 1073 K.

$$Ce_{Ce}^{\times} + 2O_O^{\times} \Leftrightarrow Ce_{Ce}' + 2V_O^{\bullet\bullet} + 3e^- + O_2 \tag{11}$$

The conduction in air, N_2 atmosphere and H_2O/H_2 atmosphere is based on the migration of oxide ions + holes, oxide ions and oxide ions + electrons, respectively. The contribution of protons to the conductivity in H_2O/H_2 atmosphere was not analyzed in this study.

Fig. 10 shows the conductivity of GDC electrolyte as a function of oxygen partial pressure at 973 and 1073 K. The electronic conductivity of LDC as calculated by the Hebb–Wagner method at 973 K[3] is also plotted in Fig. 10. The AC total conductivity and DC conductivity at 1 V in $-15 < \log P_{O_2}\,(\mathrm{Pa}) < 0$ are interpreted by the migration of oxide ions. The increase of conductivity in H_2O/H_2 atmosphere was due to the formation of electrons as a result of the dissociation of H_2 fuel in GDC electrolyte. The electronic conductivity at 973 K as calculated by the Hebb–Wagner method when the atmosphere contained no H_2 molecules was lower than the conductivity in H_2O/H_2 atmosphere. On the other hand, the AC conductivity in air at 1073 K decreased when compared with N_2 atmosphere. This is explained by Eqs. (6) and (7) in Section 3.1: (1) oxygen molecules react with oxide ion vacancies to form lattice oxide ions and holes (Eq. (6)), and (2) the formed holes oxidized Ce^{3+} to Ce^{4+} at a high temperature (Eq. (7)). The formation of Ce^{4+} ions decreases the hole concentration. Similarly, the increased reactivity between the oxide ion vacancy and the oxygen molecules reduces the con-

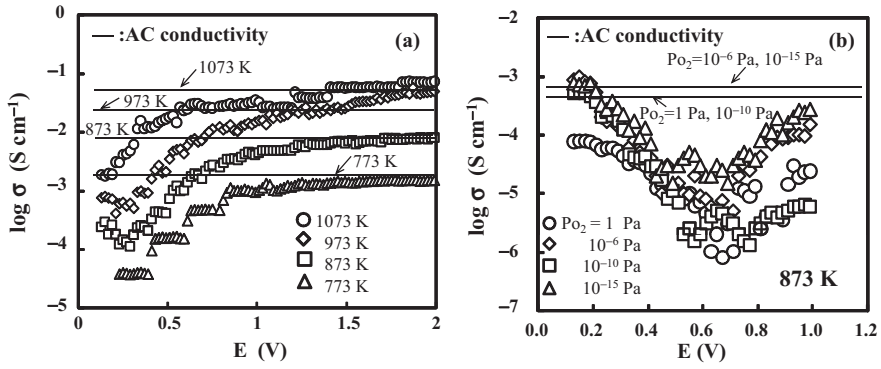

Fig. 8. Electrical conductivity–applied voltage relation for GDC in (a) air and (b) N_2 atmosphere.

centration of the oxide ion vacancy. The above reactions lead to a decrease of both hole conduction and oxide ion conduction. In a reduced atmosphere, the oxide ion vacancy concentration is increased because of the low reactivity between oxide ion vacancy and oxygen molecules, which lead to the increased oxide ion conductivity seen in N_2 atmosphere.

As seen in Figs. 9 and 10, the conductivity of GDC electrolyte is higher in H_2O/H_2 atmosphere than in N_2 atmosphere owing to the dissociation effect of H_2 molecules dissolved in GDC electrolyte ($H_2 \rightarrow 2H^+ + 2e^-$). However, the increase of electronic conduction is suppressed in $Ce_{0.9}Gd_{0.1}O_{1.95}$ electrolyte with a lower content of Gd dopant (Fig. 5). This fact is supported by the higher OCV value for a $Ce_{0.9}Gd_{0.1}O_{1.95}$ composition than for a $Ce_{0.8}Gd_{0.2}O_{1.9}$ composition.

4. Conclusions

The OCV of a GDC cell using H_2 fuel decreased as the thickness of the electrolyte became thinner. A $(La_{0.8}Sr_{0.2})(Co_{0.8}Fe_{0.2})O_3$ cathode provided a higher OCV than a $SrRuO_3$ cathode, which indicated there was a decrease of internal short circuit current (flux of oxide ions and electrons) of mixed conductor in an open circuit. The suppression of electronic conduction and the increase of oxide ion flux in the GDC electrolyte, which are achieved by using a $(La_{0.8}Sr_{0.2})(Co_{0.8}Fe_{0.2})O_3$ cathode and GDC electrolyte with a lower content of Gd dopant ($Ce_{0.9}Gd_{0.1}O_{1.95}$), enhance the OCV, leading to an increase in power density. The electrical conductivity of GDC electrolyte ($Ce_{0.8}Gd_{0.2}O_{1.9}$) is independent of oxygen partial pressure in the range of 10^{-15}–10^{0} Pa in N_2 atmosphere at 873–1073 K. Oxide ion conduction is the dominant conduction mechanism. The conductivity in H_2O/H_2 atmosphere in an oxygen partial pressure of 10^{-18} Pa at 873 K and 1073 K increased when compared with N_2 atmosphere. The increase in conductivity is due to the formation of electrons by the dissolution of hydrogen into the GDC electrolyte ($H_2 \rightarrow 2H^+ + 2e^-$). The hole conduction was observed at 873 K in an oxygen partial pressure range of 10^{0} Pa to 10^{4} Pa. The hole conduction decreased at 1073 K because of the reaction of Ce^{3+} ions with holes ($h^\bullet + Ce^{3+} \rightarrow Ce^{4+}$). The above results are closely related to the performance of a GDC cell. An appropriate selection of cathode material (LSCF) and controlling the amount of Gd dopant ($Ce_{0.9}Gd_{0.1}O_{1.95}$) are effective means for suppressing electronic conduction and for increasing the oxide ion flux in GDC electrolyte, increasing electric power density.

References

1. Jacobson AJ. Materials for solid oxide fuel cells. *Chem Mater* 2010;**22**(3):660–74.
2. Orera A, Slater PR. New chemical systems for solid oxide fuel cells. *Chem Mater* 2010;**22**(3):675–90.
3. Shimonosono T, Hirata Y, Sameshima S, Horita T. Electronic conductivity of La-doped ceria ceramics. *J Am Ceram Soc* 2005;**88**(8):2114–20.
4. Yahiro H, Eguchi K, Arai H. Electrical properties and reducibilities of ceria-rare earth oxide systems and their application to solid oxide fuel cell. *Solid State Ionics* 1989;**36**(1–2):71–5.
5. Inaba H, Tagawa H. Ceria-based solid electrolytes. *Solid State Ionics* 1996;**83**(1–2):1–16.
6. Eguchi K. Ceramic materials containing rare earth oxides for solid oxide fuel cell. *J Alloys Compd* 1997;**250**(1–2):486–91.
7. Nagamori M, Shimonosono T, Sameshima S, Hirata Y, Matsunaga N, Sakka Y. Densification and cell performance of gadolinium-doped ceria (GDC) electrolyte/NiO-GDC anode laminates. *J Am Ceram Soc* 2009;**92**(S1):S117–21.
8. Hirata Y, Matsumoto K, Sameshima S, Matsunaga N, Nagamori M, Shimonosono T. Cell performance of strontium ruthenium oxide cathode/Gd-doped ceria (GDC) electrolyte/nickel-GDC anode system. *J Ceram Soc Jpn* 2009;**117**(11):1141–6.
9. Ding C, Lin H, Sato K, Hashida T. Synthesis of NiO–$Ce_{0.9}Gd_{0.1}O_{1.95}$ nanocomposite powders for low-temperature solid oxide fuel cell anodes by co-precipitation. *Scripta Mater* 2009;**60**(4):254–6.
10. Higashi K, Sonoda K, Ono H, Sameshima S, Hirata Y. Synthesis and sintering of rare-earth-doped ceria powder by the oxalate coprecipitation method. *J Mater Res* 1999;**14**(2):957–67.
11. Shimonosono T, Hiramatsu G, Hirata Y, Sameshima S, Matsunaga N, Doi T, Horita T. Electrochemical properties of cathode for solid oxide fuel cell. *Key Eng Mater* 2007;**352**:255–8.
12. Shimonosono T, Hirata Y, Ehira Y, Sameshima S, Horita T. Electronic conductivity measurement of Gd- and Sm-doped ceria ceramics by Hebb–Wagner method. *J Ceram Soc Jpn* 2004;**112**(5):S616–21.
13. Burroughs P, Hammett A, Orchard AF, Thornton GJ. Satellite structure in the X-ray photoelectron spectra of some binary and mixed oxides of lanthanum and cerium. *J Chem Soc Dalton Trans* 1976;**17**:1686–98.
14. Sameshima S, Hirata Y, Ehira Y. Structural change in Sm- and Nd-doped ceria under a low oxygen partial pressure. *J Alloys Compd* 2006;**408-41**:628–31.
15. Hibino T, Hashimoto A, Asano K, Yano M, Suzuki M, Sano M. An intermediate-temperature solid oxide fuel cell providing higher performance with hydrocarbons than with hydrogen. *Electrochem Solid-State Lett* 2002;**5**(11):A242–4.
16. Hara A, Hirata Y, Sameshima S, Matsunaga N, Horita T. Grain size dependence of electrical properties of Gd-doped ceria. *J Ceram Soc Jpn* 2008;**116**(2):291–7.